Physica Medica 67 (2019) 1–8

Contents lists available at ScienceDirect

Physica Medica

journal homepage: www.elsevier.com/locate/ejmp

Original paper

# Electron modulated arc therapy (EMAT) using photon MLC for postmastectomy chest wall treatment I: Monte Carlo-based dosimetric characterizations

Chaoqiong Ma[a,b], David Parsons[b], Mingli Chen[b], Steve Jiang[b], Qing Hou[a], Xuejun Gu[b], Weiguo Lu[b,*]

[a] Key Lab for Radiation Physics and Technology of Education Ministry of China, Institute of Nuclear Science and Technology, Sichuan University, Chengdu, Sichuan 610064, China
[b] Department of Radiation Oncology, University of Texas Southwestern Medical Center, Dallas, TX 75235, USA

ARTICLE INFO

*Keywords:*
Electron arc therapy (EAT)
Photon MLC (pMLC)
Electron modulated arc therapy (EMAT)
Monte Carlo (MC)

ABSTRACT

*Purpose:* To study the dosimetric properties of electron arc beams delivered by photon-beam multi-leaf collimators (pMLC) in electron modulated arc therapy (EMAT) for postmastectomy chest wall treatments.
*Methods:* Using the Monte Carlo method, we simulated a 2100EX Varian linear accelerator and verified the beam models in a water tank. Dosimetric characterizations were performed on cylindrical water phantoms of elliptical bases with various field sizes, arc ranges and source-to-surface distances (SSDs) for 6, 9 and 12 MeV beam energy.
*Results:* The arc beam has a higher bremsstrahlung dose than the static beam at the isocenter due to crossfire, but choosing a field size greater than 5 cm effectively reduces the bremsstrahlung dose. The depths of the 90% maximum dose located at 1.7, 2.8 and 4.1 cm for 6, 9 and 12 MeV, respectively, are similar to those of the static beams and independent of the field size and arc range.
*Conclusion:* Based on the study, we recommend using the 5 cm field width for electron arc beams considering both bremsstrahlung dose at the isocenter and the arc profile penumbra. To ensure sufficient PTV edge coverage, we recommend a field length extension of at least 4 cm from PTV's edge for all beam energies and an arc extension of around 7°, 5°, and 5° for beam energies 6, 9, and 12 MeV, respectively. These dosimetric characterizations are the basis of pMLC-delivered EMAT treatment planning for postmastectomy chest wall patients.

## 1. Introduction

Electron therapy has played an important role in radiation therapy for the past several decades because of the advantage of the well-defined superficial dose range compared to photon therapy. With the average energy loss of ~2 MeV·cm$^2$/g in the entire beam range in water-like tissues [1,2], clinical electron beam energies are typically selected from 6 to 20 MeV when used in treating superficial targets (within 5 cm of the patients' surface), including head and neck, postmastectomy chest wall, ribs and limbs [3]. These treatment objectives are to cover the planning target volume (PTV) within the 90% isodose while minimizing the dose to adjacent and distal normal tissues [3].

In conventional electron conformal therapy, single or multiple static electron beams are typically applied by limiting the field shape to the beam's eye view of the target [3]. However, for large curved superficial PTVs, such as in the case of postmastectomy chest wall patients, a single static electron field is insufficient to cover the target; multiple fields are used to provide target coverage but may result in unacceptable dose gaps and non-uniformity at the field junctions [4]. Thus, techniques, such as electron arc therapy (EAT) [4] and modulated electron radiotherapy (MERT) [5] have been developed to improve target dose conformity and homogeneity.

Electron arc therapy (EAT), which rotationally delivers a collimated narrow beam around the PTV, was developed to reduce the hot, cold spots from adjoining static fields and dose to normal tissues for these cases [4,6–8]. However, due to potential collisions, standard applicators for static beams were replaced by secondary collimators, such as aluminum blocks, custom blocks, and multi-vane collimators, inserted on the accessory tray as well as tertiary collimators laying on the patient for edge sharpening [6,9]. These custom collimations require

* Corresponding author.
*E-mail address:* Weiguo.Lu@utsouthwestern.edu (W. Lu).

https://doi.org/10.1016/j.ejmp.2019.10.018
Received 27 June 2019; Received in revised form 2 October 2019; Accepted 3 October 2019
Available online 10 October 2019

laborious manufacturing and time-consuming, physics-demanding treatment planning; thus these techniques have been implemented only in few clinics despite the report of favorable treatment outcomes [8].

Rodrigues et al. [10] proposed dynamic arc radiation therapy (DEAR), a non-coplanar version of EAT, which uses synchronized gantry rotation, couch motion, and dose rate modulation to improve dose conformity; however, with a more complicated source trajectory and still with an electron applicator, the challenge of collision may be even greater.

In contrast to EAT, modulated electron radiotherapy (MERT) combines multiple segmented fields at fixed beam angles to create intensity modulation [5,11]; dose conformality in the depth direction is achieved by modulating electron incident energy [12–14] or using a custom bolus to modify beam penetration [15–19]. Except using the bolus for energy modulation, MERT and EAT are analogous to intensity modulated radiotherapy and volumetric modulated arc therapy in photon therapy. Multiple cutouts, dedicated electron multi-leaf collimators (eMLC), or few-leaf electron collimator (FLEC), have been implemented to create segmented fields in MERT [5,20–22], but the involved workload, dosimetry, and treatment planning remain a challenge. The built-in photon MLC (pMLC) of a linear accelerator (LINAC), on the other hand, is an attractive workaround since no custom molding to create segmented fields or independent hardware control as in eMLC or FLEC is needed. pMLC has been investigated for its dosimetric feasibility [23,24] and characterizations [25] in MERT, including treatment planning for various treatment sites [12,13,26].

The use of pMLC in EAT has also been investigated for segmented arcs [27] but with inferior dose uniformity and penumbra compared to applicator collimation due to adjoining segments and air gaps. However, using pMLC in a continuous arc may still be dosimetrically feasible, in particular, when combined with bolus modulation. Despite the interest in using pMLC, systematic dosimetric characterizations of pMLC-delivered electron arc beams are lacking. The purpose of this study is to characterize the dosimetry of electron arc beams delivered through pMLC for various beam energies, field sizes, arc ranges and source-to-surface distances (SSDs), using Monte Carlo simulations. Such characterizations allow us to identify the capabilities and limitations of pMLC-delivered electron arc beams and are the basis for selecting these parameters in electron modulated arc therapy (EMAT) treatment planning.

## 2. Methods and materials

### 2.1. Monte Carlo simulations

Electron dose distributions were simulated using the EGSnrc Monte Carlo software toolkit [28]. A 2100EX linac with a 120 leaf MLC (NDS120, Varian Medical Systems, Inc., Palo Alto, CA) was modeled in BEAMnrc [29] with exact geometric and material specifications provided by the manufacture. The model was previously validated for 6 MV photons [30–32] and updated to include 6, 9 and 12 MeV electron beams. The default parameters were used for EGSnrc with a global electron and photon cut-off energy of 521 and 10 keV, respectively. Approximately $10^8$ particles were used such that the dose uncertainty was less than 1% at the depth of the maximum dose for the chosen voxel size. The models were validated through central-axis percent depth dose (PDD) and off-axis dose ratio profile measurements acquired using a $50 \times 50 \times 50\ cm^3$ water tank (Blue Phantom 2, IBA Dosimetry GmbH, Schwarzenbruck, Germany) and a diode (60017, PTW Freiburg GmbH, Freiburg, Germany) and compared to simulated PDD using DOSXYZnrc [33] with an *xyz* voxel resolution of $4 \times 4 \times 2\ mm^2$. The *xy*- dimensions composed the transverse planes, on which the depth dose profiles were evaluated, and the *z*-dimension was in the longitudinal direction, along which the in-plane profiles were evaluated. The electron beam measurements were performed by overriding the applicator interlock [27]. The electron energy was tuned to match PDD, and the scattering foils was tuned to match profiles [34] for the $30 \times 30\ cm^2$ field, without deviating too far from manufacturer's specification, and validated by multiple rectangular fields of static beams.

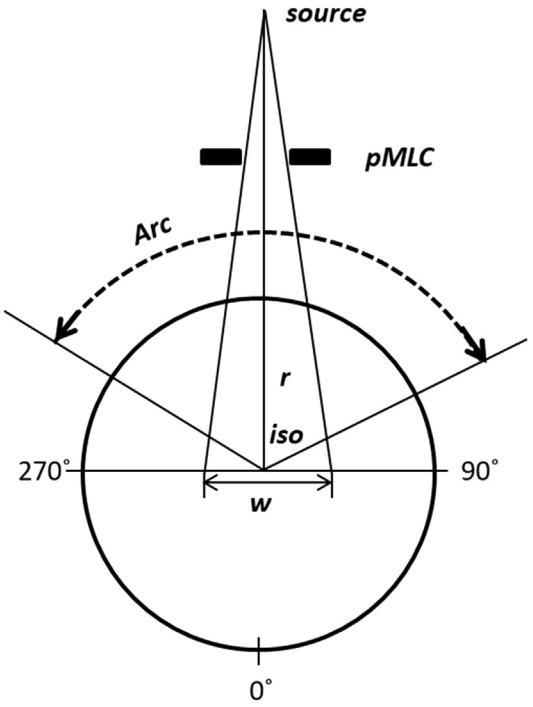


**Fig. 1.** Schematic illustration of beam geometry on a transverse plane of a cylindrical phantom with radius *r* and field width *w*.

Electron arc treatments were simulated using source 20 in DOSXYZnrc developed by Lobo et al. [31]. The arcs were simulated using one-degree resolution for the calculation purpose; physical delivery would be continuous rotation. EGSPHANT files were created to simulate various regular and elliptical cylinders with an *xyz* voxel resolution of $1 \times 1 \times 4\ mm^3$. For arc delivery, both the depth dose and arc profiles are evaluated on the central transverse plane.

### 2.2. Electron arc beams collimated by pMLC

The electron arc beam dose was calculated on cylindrical water phantoms, including circular and elliptical-based cylinders, for dosimetric characterizations. The arc delivery and circular-based cylindrical phantom are illustrated in Fig. 1. The radiation isocenter was selected at the cylinder center, and the field width and length were defined at the isocenter plane.

Photon MLCs were used to shape rectangular fields, and the coordinates were defined using the IEC 61217 system. Unless stated otherwise, all simulations used the 180° electron arc clockwise from gantry angle 270° to 90° (Fig. 1), the $5 \times 30 cm^2$ field, the cylinder with radius of 15 cm and length of 40 cm, and the fixed source-to-axis distance (SAD) of 100 cm. Depth dose in the radial direction at the arc center (radial PDD), arc dose on the transverse plane, and longitudinal dose in the cylinder axes direction were analyzed for combinations of beam energies, field sizes, arc ranges and cylinder radii. Table 1 lists the parameters of combinations. As clinical electron treatment plans are required to cover the PTV by the 90% isodose, all arc and longitudinal dose profiles were evaluated at $R_{90}$, the depth of 90% maximum dose, of the radial PDD and normalized to the maximum dose. Here $R_n$ denotes the depth of *n*% maximum dose on the electron percent depth dose (PDD) curve. For example, $R_{100}$ is the depth of (100%) maximum dose.

**Table 1**
Parameters for the dosimetric characteristic study. Combinations of these parameters were used to study the effect of beam energy, field size, arc range, and SSD. The value pairs of elliptical cylinders indicate the major and minor axes.

| | |
|---|---|
| Beam energy (MeV) | 6, 9, 12 |
| Field width (cm) | 3, 5, 7 |
| Field length (cm) | 10, 20, 30 |
| Arc range (°) | 60, 120, 180 |
| Cylinder radius (cm) | 10, 15, 20 |
| Elliptical cylinder (cm) | (20,10), (20,15) |

#### 2.2.1. Beam energy effect

We chose 6, 9 and 12 MeV beam energies because they are close to the energy for chest wall treatments and because higher energy beams are associated with higher bremsstrahlung dose and longer beam ranges causing adjacent OARs to receive more radiation dose. We investigated the beam energy effect on the depth dose at the center of the 180° arc by varying the beam energy but fixing the field size and phantom dimensions.

#### 2.2.2. Field size effect

The dosimetric effect of field size was studied using rectangular fields, where the field width is the collimation width along the arc and the field length is determined by the superior-inferior target coverage. To reduce the effect of oblique electron beam incidence that results in large dose deviation from normal incidence [35], small field widths, 3, 5, and 7 cm, were selected for electron arc beams. Radial PDDs and arc dose profiles were studied for the field width effect. The effect of field length was studied by comparing longitudinal dose profiles of three field lengths, 10, 20, and 30 cm.

#### 2.2.3. Arc range effect

We varied the arc range from 60° to 180° to simulate a range of irradiation from ipsilateral chest wall to bilateral chest wall. The effect of arc range on the radial PDDs and arc dose profiles was analyzed.

#### 2.2.4. Source-to-surface distance (SSD) effect

The effect of chest wall SSD was investigated on radial PDDs, arc and longitudinal dose profiles using various cylinder radii, 10, 15, and 20 cm, and elliptical cylinders with a major axis of 20 cm and minor axis of 10 and 15 cm in three beam energies, 6, 9, and 12 MeV. Since the SAD was fixed at 100 cm, the cylinder radii of 10, 15, and 20 cm corresponded to the SSD of 90, 85, and 80 cm, respectively. We compared the dose distributions of regular and elliptical cylinders to create a more contrasting view of the SSD effect.

## 3. Results

### 3.1. Monte Carlo validation

The measured and simulated PDDs at the center of the field $30 \times 30$ cm$^2$ agreed within 2% for energies 6, 9 and 12 MeV (Fig. 2). The profiles at $R_{90}$ (Fig. 3) similarly agreed within 2% in the central region and within 2.5 mm in the gradient, corresponding to an energy uncertainty of approximately 0.5 MeV. Similar agreement was found for the validation fields. Fig. 4 shows the results of the $30 \times 3$ cm$^2$.

The simulation time with EGSnrc was ~30 min and ~1% statistical uncertainty on a 14-core computer.

### 3.2. Dosimetric characteristics of electron arc beams collimated by pMLC

#### 3.2.1. Beam energy effect

The radial PDDs of different beam energies are shown in Fig. 5. The surface doses were 68%, 65%, and 62%, for 6 MeV, 9 MeV and 12 MeV, respectively. This contrasted with static beams: the surface dose for static beams of the same field $5 \times 30$ cm$^2$ were 74%, 78%, and 85% for 6 MeV, 9 MeV and 12 MeV, respectively. This contrast was due to the increased irradiation time (dose rate) with respect to the increased depth in arc delivery, also known as the $\beta$ angle effect [36]. The depths $R_{100}$, $R_{90}$ and $R_{20}$, like those of the static beam, increased as the energy increased. They also increased slightly relative to those of the static beam due to the $\beta$ angle effect. The falloff distance increased, or equivalently, the gradient decreased between $R_{90}$ and $R_{20}$ ($R_{90-20}$) with increased energy: $R_{90-20}$ increased from 0.9 to 1.7 cm as the beam energy increased from 6 MeV to 12 MeV (Table 2). Finally, the bremsstrahlung dose peaked near the isocenter were 2%, 4% and 8% for 6, 9, and 12 MeV electron arc beams, respectively.

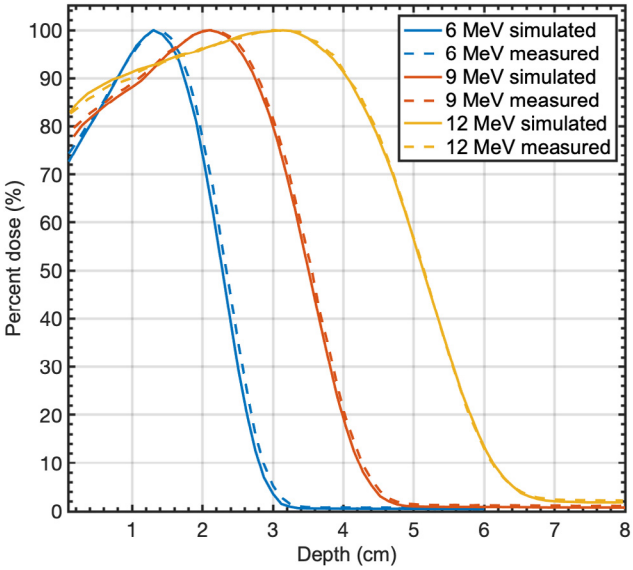


**Fig. 2.** Measured and simulated PDDs with a field size of $30 \times 30$ cm$^2$ for energies 6, 9 and 12 MeV.

#### 3.2.2. Field size effect

The radial PDDs of field widths 3, 5, and 7 cm for each of the three beam energies, 6, 9, and 12 MeV are shown in Fig. 6. For the same energy, there was no significant difference in PDDs of different field widths until the depth reaches 10 cm, where the bremsstrahlung dose becomes prominent. The bremsstrahlung dose (%) at the isocenter increases as the field width decreases (Table 3) due to the crossfire effect and is consistent with the work of Leavitt et al. [6] and Pla et al. [37]. Here the crossfire effect refers to that the isocenter is always under irradiation since it is the focus of all beams in rotational delivery. In fact, all points that are within half the field width from the isocenter will be irradiated all the time in rotational delivery, and as the field width decreases, the crossfire effect increases.

The effect of field width on arc dose is shown in Fig. 7 for 9 MeV. The ramp (dose falloff) is centered at the 90° angle and extends about 15° angle on each side of the center, which can potentially impacts dose conformity and homogeneity. There is a slight effect of field width and beam energy on the falloff gradient. The smaller field and higher energy correspond to the slightly steeper dose falloff shown in Table 4 as seen by the angle of the 80% maximum dose, $A_{80}$, and the degree arc from the 80% to 20% maximum dose, $A_{80-20}$.

The longitudinal dose profiles at the depth $R_{90}$ along the arc center are shown in Fig. 8 for the 10, 20 and 30 cm field length for the 9 MeV beam. The dose falloff measured at the 80% maximum dose, $L_{80}$, and distance between 80% and 20% maximum dose, $L_{80-20}$, are listed in Table 6 for different field lengths for each beam energy.

As the energy increased from 6 MeV to 12 MeV, $L_{80}$ increased slightly from 2.3 cm to 2.7, from 6.4 cm to 7.3 cm, and from 11.1 cm to 11.7 cm, for field length 10 cm, 20 cm, and 30 cm, respectively. Higher

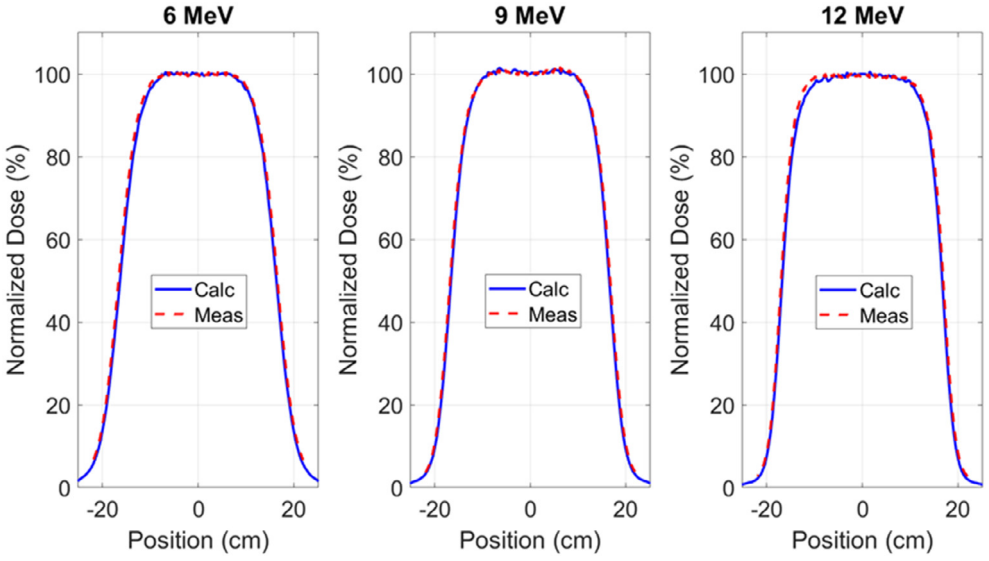


**Fig. 3.** Measured and simulated in-plane profiles at $R_{90}$ with a field size of 30 × 30 cm$^2$ for energies 6, 9 and 12 MeV.

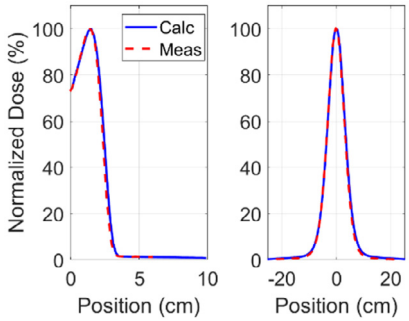


**Fig. 4.** Measured and simulated PDDs and in-plane profiles with a field size of 30 × 3 cm$^2$ for the 6 MeV electron beam.

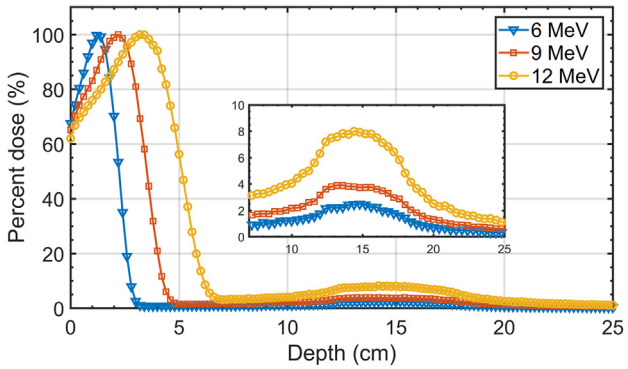


**Fig. 5.** Radial PDDs of 180° electron arc beams with the 5 × 30 cm$^2$ field for 6, 9 and 12 MeV beam energies.

**Table 2**
Depth dose positions $R_{100}$, $R_{90}$ and $R_{20}$ in unit of cm for a 5 × 30 cm$^2$ field, 180° arc, and 6, 9 and 12 MeV beam energy. In parentheses are those of static beams of the same field size.

| Beam energy (MeV) | $R_{100}$ | $R_{90}$ | $R_{20}$ |
|---|---|---|---|
| 6 | 1.3 (1.4) | 1.7 (1.8) | 2.6 (2.7) |
| 9 | 2.2 (2.1) | 2.8 (2.8) | 4.0 (4.0) |
| 12 | 3.3 (3.1) | 4.1 (4.0) | 5.8 (5.7) |

energy yielded slightly sharper penumbra, which enables higher dose homogeneity for the same normal tissue toxicity constraint. $L_{80-20}$ increased by approximately 4 mm as field length increased from 10 cm to 30 cm for the same energy; that is, dose fall-off along the longitudinal direction was marginally sharper with smaller field lengths.

### 3.2.3. Arc range

No significant difference was observed in the PDD curves, except for the bremsstrahlung dose near the isocenter. Fig. 9 illustrates the variation in bremsstrahlung dose component for various arc ranges. Dose at the isocenter increased by 1.3%, 2.4% and 5.0% for 6 MeV, 9 MeV and 12 MeV, respectively, as the arc range increased from 60° to 180°.

### 3.2.4. Source-to-surface distance

Fig. 10 shows the radial PDDs of the 12 MeV beam for different phantom radii (therefore, different SSD). In Fig. 10a, each curve is normalized by its own maximum. There was no significant difference in $R_{100}$, $R_{90}$ and $R_{90-20}$, but surface dose increased as the radius increased, with a maximum increase of 13% between the 10 cm and 20 cm phantom radii. Also, the bremsstrahlung dose at the isocenter increased with increased phantom radii. In contrast, the curves in Fig. 10b are normalized by the maximum dose of the phantom of 10 cm radius. The increased dose with decreased radius is due to the increased irradiation time toward the isocenter, while the increased bremsstrahlung dose with decreased radius is due to decreased attenuation.

Fig. 11(a) and (b) illustrate arc and longitudinal dose profiles at $R_{90}$, respectively, for phantom radii 10 cm, 15 cm and 20 cm at 12 MeV, with specific values of $A_{80}$, $A_{80-20}$ listed in Table 5 and $L_{80}$, $L_{80-20}$ in Table 6. The penumbra increases as the phantom radius decreases, due to the divergence effect.

Fig. 12 illustrates the dose distributions at the central transverse planes of elliptical cylindrical phantoms with the same major axis 20 cm but different minor axes 10 cm, 15 cm and 20 cm, for 9 MeV beam with a fixed field size 5 × 30 cm$^2$ and arc range 360°. Surface dose increased as surface-to-isocenter distance decreased.

## 4. Discussion

In this work, we characterized pMLC-delivered electron arc beam dosimetry through investigating three dose profiles, radial PDD, arc profiles, and longitudinal profiles, on various circular and elliptical-based cylindrical phantoms, for various beam parameters based on Monte Carlo (MC) simulations validated for statics beams. Though we

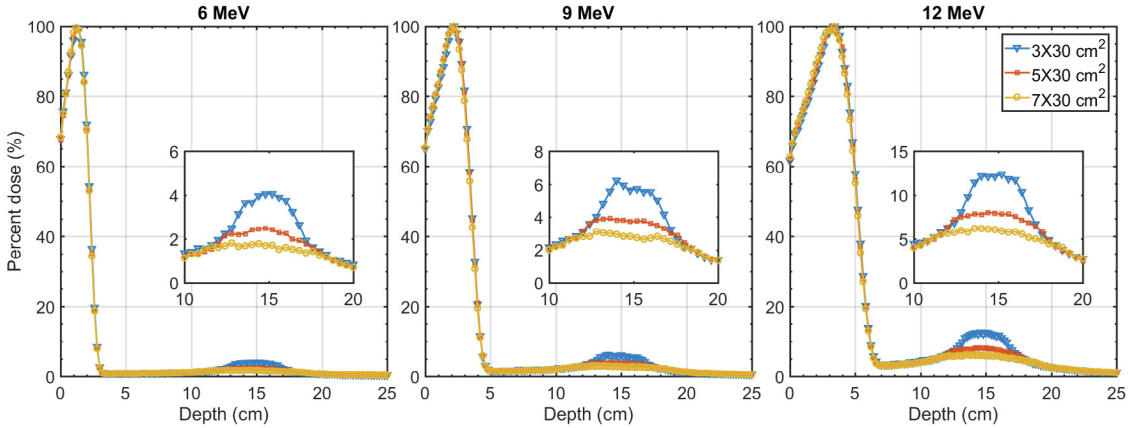


**Fig. 6.** Radial PDDs of 180° electron arc beams with field widths of 3, 5, and 7 cm for each of the three beam energies, 6 MeV (left), 9 MeV (middle), and 12 MeV (right).

**Table 3**
Dose (%) at the isocenter for field width 3, 5 and 7 cm, beam energy 6, 9 and 12 MeV, and electron arc 180°.

| Beam energy (MeV)\ Field width (cm) | 3 | 5 | 7 |
|---|---|---|---|
| 6 | 3.9 | 2.3 | 1.8 |
| 9 | 6.0 | 3.8 | 2.9 |
| 12 | 12.5 | 8.1 | 5.9 |

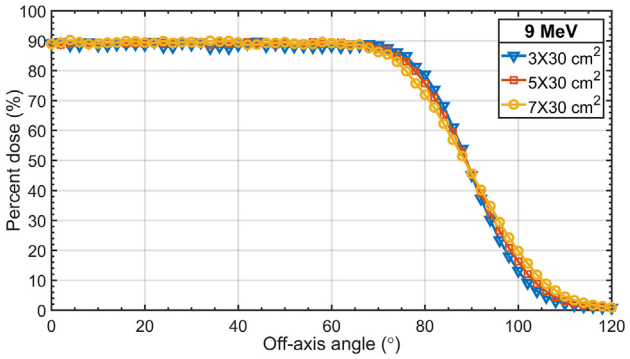


**Fig. 7.** Arc dose profiles at $R_{90}$ for field width of 3 cm, 5 cm and 7 cm for 180° arc beams of energy 9 MeV. Only half the profiles are shown due to symmetry about 0°. The $x$-axis is the angle (°) from the center of the arc.

**Table 4**
$A_{80}$ and $A_{80-20}$ (in parentheses) of the arc dose profiles at widths of 3 cm, 5 cm and 7 cm for 180° electron arc beams of energies 6 MeV, 9 MeV and 12 MeV. All values are in units of degree (°).

| Beam energy (MeV)\ Field width (cm) | 3 | 5 | 7 |
|---|---|---|---|
| 6 | 78 (20) | 76 (23) | 75 (24) |
| 9 | 79 (18) | 78 (21) | 76 (24) |
| 12 | 80 (18) | 78 (20) | 76 (23) |

did not measure the electron arc beams, the MC-simulated radial PDD were similar to those measured by Leavitt et al. [6] (Fig. 5 therein). For the same geometry and setup as ours (5-cm field width, 100-cm SAD, 15-cm cylinder radius, 180° arc), except that they used aluminum secondary collimators mounted on an acrylic accessory tray insert instead of pMLC, their measured surface dose were 70%, 67%, and 68%, and $R_{100}$ were 1.3 cm, 2.2 cm, and 3.3 cm, approximately, for 6, 9, and 12 MeV, respectively (by visual inspection of their graphs). Our simulated $R_{100}$ agreed with their measurements, but surface dose was slightly lower at 68%, 65%, and 62%, for 6, 9, and 12 MeV, respectively

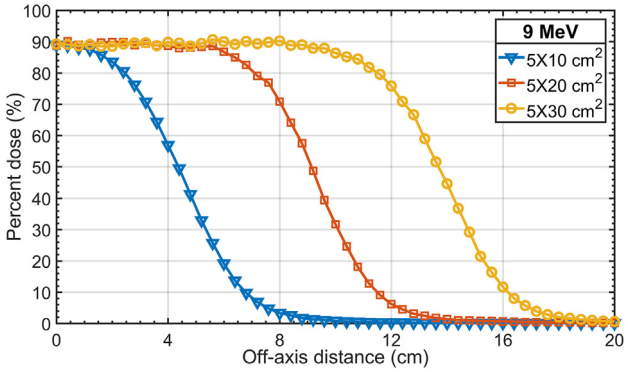


**Fig. 8.** Longitudinal dose profiles at $R_{90}$ (defined at the arc center) with field lengths of 10 cm, 20 cm and 30 cm for 180° electron arcs at 9 MeV. Only half the profiles are shown due to symmetry.

(Fig. 5). The slightly lower surface dose in our simulations may be accounted for by the greater clearance between pMLC and patient surface that fewer low energy scattered electrons reach the phantom surface [6].

The electron arc beam can be regarded as a superposition of static beams, and difference of dosimetric characteristics between the arc and static beams can be largely attributed to the radial dose rate property. The dose rate increases as the radial depth increases due to the crossfire effect and saturates at depth within the field from all beam angles, i.e. where the distance from the rotation axis is less than one half field width. Such radial dose rate property has been observed by Khan et al. [4] and Pla et al. [36]. Khan et al. explained this as a mechanism of angular velocity, in which as depth increases, linear velocity decreases, thereby increasing the apparent exposure time to the beam. Pla et al. described this by the $\beta$-angle concept, i.e. the arc range of radiation exposure, and the inverse square law of the divergence effect; however, the latter has only a second order effect for typical treatment SADs. The $\beta$-angle ratio (dose rate ratio) against radial position for multiple field widths are illustrated in Fig. 13.

The radial dose rate property causes the surface dose of the electron arc beam to be lower than that of the static beam when all other beam parameters are fixed. Similarly, $R_{100}$ is increased due to the increased dose rate along the depth. These effects are more substantial at higher energy since the $R_{100}$ of higher energy beam is at a deeper location, causing the surface dose (%) to decrease as the beam energy (6, 9, and 12 MeV) increases, which exactly reverses the order of surface dose (%) with static beams (Fig. 2).

The higher surface doses near the minor axis than those near the major axis for elliptical cylinders can be explained by the same reason,

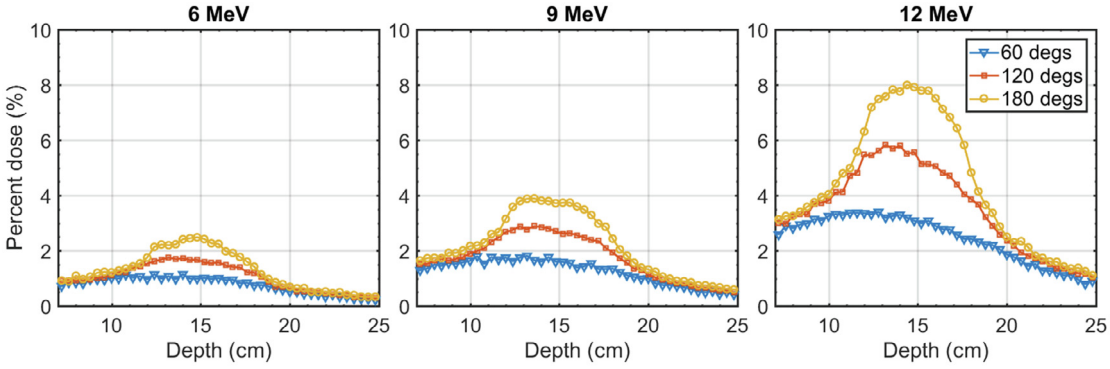


**Fig. 9.** Bremsstrahlung radial PDD component at arc ranges of 60°, 120° and 180° for 6 MeV (left), 9 MeV (middle) and 12 MeV (right).

which is commonly referred to as the SSD effect but can be more directly expressed as the effect of the distance to the rotation axis. The doses of elliptical cylinders, like those of the chest wall, were also affected by electron beam incidence obliquity, but the obliquity effect was small since the selected field widths were small. Furthermore, with a properly selected isocenter, the obliquity effect can also be reduced [38].

In addition to the increased practical range with energy, the bremsstrahlung component, which occurs within 3 cm from the rotation axis in all simulations, was amplified. This could be problematic for chest wall treatments, where the PTV distal edges are adjacent to the lung tissue. In these cases, a large amount of lung volume would be exposed to radiation with high energy (≥12 MeV) arc beams due to the low density of the lung tissue (approximately one-fifth of water). Therefore, the use of high energy (≥12 MeV) electron arcs for chest wall irradiations requires extra attention to avoid excessive dose to lungs.

The arc and longitudinal dose profiles were studied at $R_{90}$, and the profile penumbra were evaluated using 80% and 20% maximum dose. The profile penumbra is relevant in treatment planning since the steeper penumbra enables higher dose conformity and homogeneity. We found that the beam energy has a slight effect on the penumbra of the arc and longitudinal dose profiles: the higher energy, the sharper penumbra with an effect of ~5 mm or less.

In the investigation of the field width effect, there was no significant difference in the build-up regions, $R_{100}$, $R_{90}$ and $R_{20}$ of PDDs for all three investigated field widths, 3, 5, and 7 cm, for fixed beam energies. Thus, the common $R_{90}$, 1.7 cm, 2.8 cm, and 4.1 cm, for 6 MeV, 9 MeV, and 12 MeV, respectively, can be regarded as the standard $R_{90}$ when selecting the beam energy in pMLC-based electron arc treatment planning.

On the other hand, the field width effect on the bremsstrahlung dose is prominent. The 3 cm field width yields twice as high bremsstrahlung dose as that of the 7 cm field width. In fact, the bremsstrahlung dose increases as the field width decreases, again, due to the crossfire effect, since the relative dose rate of $R_{100}$ to the center is lower for the larger field (Fig. 13). These results are consistent with those using the x and y jaws to collimate electron arc beams, where 4 to 8 cm field widths were recommended to avoid markedly higher bremsstrahlung dose of smaller field widths [6,37].

There is also a clear effect of the field size on the penumbra of the arc and longitudinal dose profiles: the penumbra increases as the field size increase with increasing effect for increasing beam energy.

Non-rectangular fields may be used in arc delivery though not studied in this work. Leavitt et al. [6] used custom collimation to create trapezoid fields for electron arc beams to generate non-uniform dose rates at different longitudinal positions. Dynamically opening/closing fields in arc delivery may be used to sharpen the penumbra and would entail the use of in-transit small fields. Klein et al. [23] and Mihaljevic et al. [39] verified Monte Carlo simulations for small fields ($1 \times 1$, $2 \times 2$, $2.6 \times 2.6$ cm$^2$) with static beams but did not recommend them for electron beams since the percentage of bremsstrahlung dose is high beyond the beam range. It would be much easier to create non-rectangular or dynamically changing fields with pMLC then with custom collimation, and their dosimetric feasibility will be studied in the future.

The arc range has minimal dosimetric effects except for the bremsstrahlung dose, which increases with the increasing arc range.

The effect of SSD is prominent in both bremsstrahlung dose and profile penumbra. Besides the radial dose rate property, the SSD also

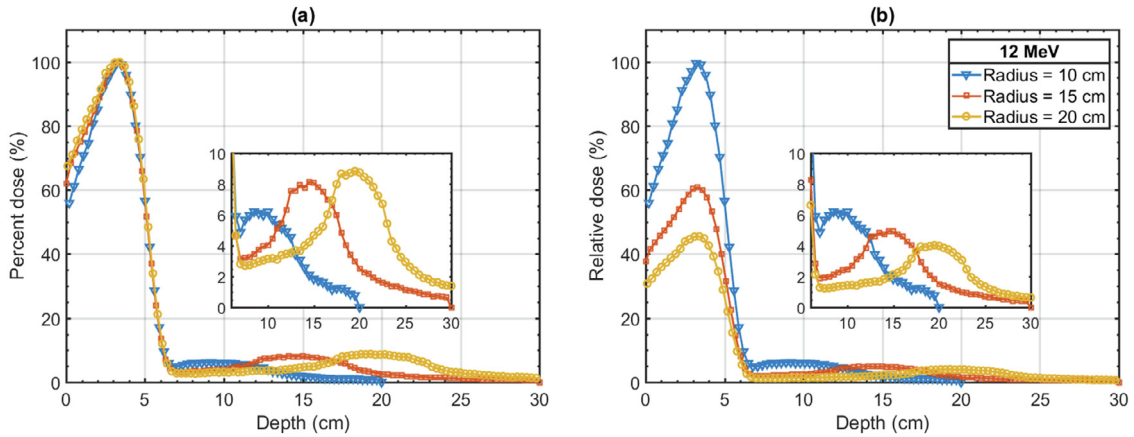


**Fig. 10.** (a) Radial PDDs (normalized by each curve's own maximum) of cylindrical phantoms of radii 10, 15 and 20 cm, corresponding to SSD of 90, 85 and 80 cm, respectively, at a fixed field size $5 \times 30$ cm$^2$ for 180° electron arc beams of energy 12 MeV; (b) Similar to (a) but normalization was by $d_{max}$ for the phantom of radius 10 cm.

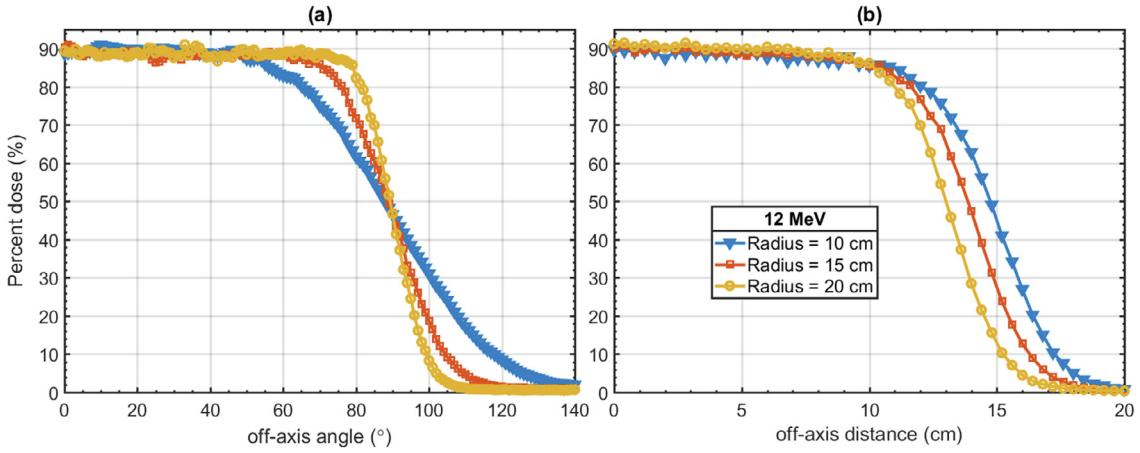


**Fig. 11.** (a) Arc dose profiles at the central transverse plane and (b) longitudinal dose profiles at the arc center, both at $d_{90}$, for cylindrical phantoms of radii 10, 15, and 20 cm, corresponding to the SSD of 90, 85, and 80 cm, respectively, of the 12 MeV beam. Only half the profiles are shown due to symmetry. In (a), The $x$-axis is the angle (°) from the center of the arc.

**Table 5**
$A_{80}$ and $A_{80–20}$ (in parentheses) for cylindrical phantoms of radii 10, 15, and 20 cm (corresponding to SSD 90, 85, and 80 cm, respectively) for 180° electron arc beams of energies of 6 MeV, 9 MeV and 12 MeV. All values are in units of degree (°).

| | 6 MeV | 9 MeV | 12 MeV |
|---|---|---|---|
| 10 cm | 68 (40) | 68 (40) | 65 (42) |
| 15 cm | 78 (26) | 78 (25) | 77 (27) |
| 20 cm | 83 (15) | 84 (14) | 85 (14) |

**Table 6**
$L_{80}$ and $L_{80–20}$ (in parentheses) for cylindrical phantoms of radiuses 10 cm, 15 cm and 20 cm (corresponding to SSD 90, 85, and 80 cm, respectively) for 180° electron arc beams of energies of 6 MeV, 9 MeV and 12 MeV. All values are in units of cm.

| | 6 MeV | 9 MeV | 12 MeV |
|---|---|---|---|
| 10 cm | 12.0 (4.6) | 12.2 (4.3) | 12.1 (4.3) |
| 15 cm | 11.1 (4.3) | 11.5 (3.8) | 11.6 (3.9) |
| 20 cm | 10.5 (3.8) | 11.0 (3.4) | 11.0 (3.5) |

has an effect on in-air scatter. The larger penumbra was observed for the smaller phantom radius due to larger scatter with the larger SSD. The extended shoulder ($L_{80}$) of the longitudinal dose profile with the small phantom radius, however, is attributed to the divergence effect.

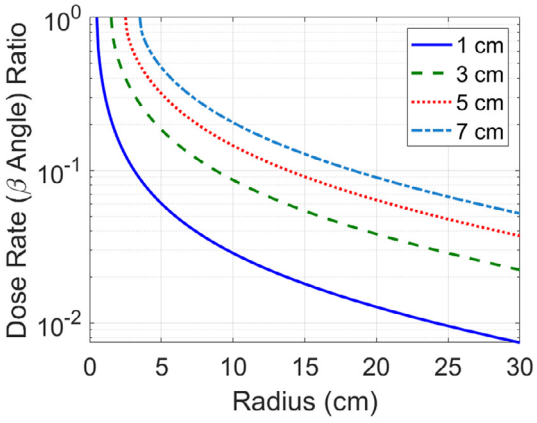


**Fig. 13.** Dose rate ratio against the radial position for field widths of 1, 3, 5, and 7 cm in electron arc beams of 180° arc.

The absolute dose was not calibrated in this work since we used the relative dose for treatment planning. To measure planning dose, the absolute dose calibration would be required, and it is possible [40]. The output needs be measured against a standard beam; currently, the standard beam is the one with $10 \times 10$ cm$^2$ cutout and SSD 105 cm. Mueller et al. [25] showed that with the same field size $9.8 \times 9.8$ cm$^2$, the output of pMLC with SSD 100 cm is similar to that of the cut-out

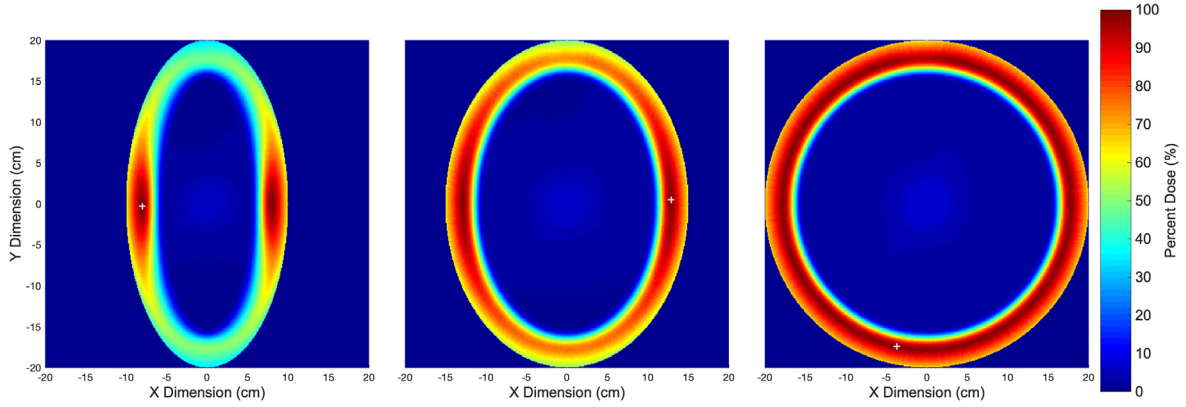


**Fig. 12.** Normalized dose distributions at the central transverse planes of the elliptical cylinders of the same major axis 20 cm but different minor axes: 10 (left), 15 (middle), and 20 cm (right) for a fixed field size $5 \times 30$ cm$^2$ and 360 electron arc beams in 9 MeV beam energy. The white cross in each image marks the normalization reference point.

with SSD 105 cm, and the output of the pMLC was nearly 3× as high when the SSD was 70 cm. Thus, the delivery time would be comparable to that of comprehensive chest wall treatments, such as Electron Arc Therapy (EAT) [7,8].

Based on the dosimetric characterizations, we recommend placing the isocenter such that the average SSD is less than 80 cm to reduce the penumbra due to air scatter and to minimize surface distance variation responsible for the hot/cold spots. Small SSD may be prohibitive because of the risk of collision between the patient and gantry. The isocenter selection is further investigated in the EMAT treatment planning study [38]. We recommend using the 5 cm field width because it marginally increases bremsstrahlung dose and penumbra compared to the 7 and 3 cm field widths, respectively. We also recommend using a field length that is at least a 4 cm extension from each end of the PTV as seen on SSD to ensure PTV end coverage by 80% isodose. Similarly, the arc extensions by 7, 5, and 5° from each end of PTV for 6, 9, and 12 MeV, respectively, are recommended. The dose falloff regions associated with the extensions will be accounted for by the bolus design in the EMAT treatment planning study [38].

## 5. Conclusion

In this work, we investigated the dosimetric characteristics of the pMLC-delivered electron arc beam. It has the potential to produce homogeneous dose distributions in the PTVs while maintaining sharp dose fall-offs with properly selected parameters. This work provides the basis of selecting arc beam parameters, including beam energy, field size, isocenter position, and arc range for chest wall treatment planning in pMLC-delivered EMAT.

## Acknowledgments

This work was partially supported by China Scholarship Council (CSC) and by NIH R01 CA218402 and R01 CA235723.

## References

[1] ICRU. Report 90. J Int Commission Radiat Unit Meas 2016;14.
[2] Strydom W, Parker W, Olivares M. Electron beams: physical and clinical aspects Chapter 8 Vienna: International Atomic Energy Agency; 2005. p. 657.
[3] Hogstrom KR, Almond PR. Review of electron beam therapy physics. Phys Med Biol 2006;51:R455–89.
[4] Khan FM, Fullerton GD, Lee JMF, Moore VC, Levitt SH. Physical aspects of electron-beam arc therapy. Radiology 1977;124:497–500.
[5] Ma CM, Pawlicki T, Lee MC, Jiang SB, Li JS, Deng J, et al. Energy- and intensity-modulated electron beams for radiotherapy. Phys Med Biol 2000;45:2293.
[6] Leavitt DD, Peacock LM, Gibbs FA, Stewart JR. Electron arc therapy: physical measurement and treatment planning techniques. Int J Radiat Oncol Biol Phys 1985;11:987–99.
[7] Leavitt DD, Stewart JR. Electron arc therapy of the postmastectomy prosthetic breast. Int J Radiat Oncol Biol Phys 1994;28:297–301.
[8] Gaffney DK, Leavitt DD, Tsodikov A, Smith L, Watson G, Patton G, et al. Electron arc irradiation of the postmastectomy chest wall with CT treatment planning: 20-year experience. Int J Radiat Oncol Biol Phys 2001;51:994–1001.
[9] Leavitt DD, Stewart JR, Moeller JH, Earley L. Optimization of electron arc therapy doses by multi-vane collimator control. Int J Radiat Oncol Biol Phys Feb 1989;16:489–96.
[10] Rodrigues A, Yin FF, Wu Q. Dynamic electron arc radiotherapy (DEAR): a feasibility study. Phys Med Biol 2014;59:327–45.
[11] Zackrisson B, Karlsson M. Matching of electron beams for conformal therapy of target volumes at moderate depths. Radiother Oncol Jun 1996;39:261–70.
[12] Salguero FJ, Palma B, Arrans R, Rosello J, Leal A. Modulated electron radiotherapy treatment planning using a photon multileaf collimator for post-mastectomized chest walls. Radiother Oncol 2009;93:625–32.
[13] Salguero FJ, Arrans R, Palma BA, Leal A. Intensity- and energy-modulated electron radiotherapy by means of an xMLC for head and neck shallow tumors. Phys Med Biol 2010;55:1413–27.
[14] Henzen D, Manser P, Frei D, Volken W, Neuenschwander H, Born EJ, et al. Beamlet based direct aperture optimization for MERT using a photon MLC. Med Phys 2014;41:121711.
[15] Low DA, Starkschall G, Bujnowski SW, Wang LL, Hogstrom KR. Electron bolus design for radiotherapy treatment planning: Bolus design algorithms: Electron bolus design for radiotherapy treatment planning. Med Phys 1992;19(1):115–24. https://doi.org/10.1118/1.596885.
[16] Kudchadker RJ, Hogstrom KR, Garden AS, McNeese MD, Boyd RA, Antolak JA. Electron conformal radiotherapy using bolus and intensity modulation. Int J Radiat Oncol Biol Phys 2002;53:1023–37.
[17] Kudchadker RJ, Antolak JA, Morrison WH, Wong PF, Hogstrom KR. Utilization of custom electron bolus in head and neck radiotherapy. J Appl Clin Med Phys 2003;4:321–33.
[18] Su S, Moran K, Robar James L. Design and production of 3D printed bolus for electron radiation therapy. J Appl Clin Med Phys 2014;15:194–211.
[19] Lukowiak M, Jezierska K, Boehlke M, Wiecko M, Lukowiak A, Podraza W, et al. Utilization of a 3D printer to fabricate boluses used for electron therapy of skin lesions of the eye canthi. J Appl Clin Med Phys 2017;18:76–81.
[20] Ravindran BP, Singh IR, Brindha S, Sathyan S. Manual multi-leaf collimator for electron beam shaping–a feasibility study. Phys Med Biol 2002;47:4389–96.
[21] Hogstrom KR, Boyd RA, Antolak JA, Svatos MM, Faddegon BA, Rosenman JG. Dosimetry of a prototype retractable eMLC for fixed-beam electron therapy. Med Phys 2004;31:443–62.
[22] Al-Yahya K, Schwartz M, Shenouda G, Verhaegen F, Freeman C, Seuntjens J. Energy modulated electron therapy using a few leaf electron collimator in combination with IMRT and 3D-CRT: Monte Carlo-based planning and dosimetric evaluation. Med Phys 2005;32:2976–86.
[23] Klein EE, Vicic M, Ma CM, Low DA, Drzymala RE. Validation of calculations for electrons modulated with conventional photon multileaf collimators. Phys Med Biol 2008;53:1183–208.
[24] du Plessis FC, Leal A, Stathakis S, Xiong W, Ma CM. Characterization of mega-voltage electron beams delivered through a photon multi-leaf collimator (pMLC). Phys Med Biol 2006;51:2113–29.
[25] Mueller S, Fix MK, Henzen D, Frei D, Frauchiger D, Loessl K, et al. Electron beam collimation with a photon MLC for standard electron treatments. Phys Med Biol 2018;63:025017.
[26] Jin L, Ma CM, Fan J, Eldib A, Price RA, Chen L, et al. Dosimetric verification of modulated electron radiotherapy delivered using a photon multileaf collimator for intact breasts. Phys Med Biol 2008;53:6009–25.
[27] Klein EE, Li Z, Low DA. Feasibility study of multileaf collimated electrons with a scattering foil based accelerator. Radiother Oncol 1996;41:189–96.
[28] Kawrakow I. Accurate condensed history Monte Carlo simulation of electron transport. I. EGSnrc, the new EGS4 version. Med Phys 2000;27:485–98.
[29] Rogers DW, Faddegon BA, Ding GX, Ma CM, We J, Mackie TR. BEAM: a Monte Carlo code to simulate radiotherapy treatment units. Med Phys 1995;22:503–24.
[30] Berbeco RI, Detappe A, Tsiamas P, Parsons D, Yewondwossen M, Robar J. Low Z target switching to increase tumor endothelial cell dose enhancement during gold nanoparticle-aided radiation therapy. Med Phys 2016;43:436.
[31] Lobo J, Popescu IA. Two new DOSXYZnrc sources for 4D Monte Carlo simulations of continuously variable beam configurations, with applications to RapidArc, VMAT, TomoTherapy and CyberKnife. Phys Med Biol 2010;55:4431–43.
[32] Parsons D, Robar JL. Beam generation and planar imaging at energies below 2.40 MeV with carbon and aluminum linear accelerator targets. Med Phys 2012;39:4568–78.
[33] Walters B, Kawrakow I, Rogers DW. DOSXYZnrc Users Manual NRCC Report PIRS-794revB. Ottawa, Canada: National Research Council; 2018.
[34] Bieda MR, Antolak JA, Hogstrom KR. The effect of scattering foil parameters on electron-beam Monte Carlo calculations. Med Phys 2001;28:2527–34.
[35] Ekstrand KE, Dixon RL. The problem of obliquely incident beams in electron-beam treatment planning. Med Phys 1982;9:276–8.
[36] Pla M, Pla C, Podgorsak EB. The influence of beam parameters on percentage depth dose in electron arc therapy. Med Phys 1988;15:49–55.
[37] Pla M, Podgorsak EB, Pla C. Electron dose rate and photon contamination in electron arc therapy. Med Phys 1989;16:692–7.
[38] Ma C, Chen M, Parsons D, Jiang S, Hou Q, Gu X. et al. Electron modulated arc therapy (EMAT) using photon MLC for postmastectomy chest wall treatment II: 3D bolus design. under consideration by PMB; 2019.
[39] Mihaljevic J, Soukup M, Dohm O, Alber M. Monte Carlo simulation of small electron fields collimated by the integrated photon MLC. Phys Med Biol 2011;56:829–43.
[40] Popescu IA, Shaw CP, Zavgorodni SF, Beckham WA. Absolute dose calculations for Monte Carlo simulations of radiotherapy beams. Phys Med Biol 2005;50:3375–92.